Electrical Power and Energy Systems 101 (2018) 1–12

Contents lists available at ScienceDirect

Electrical Power and Energy Systems

journal homepage: www.elsevier.com/locate/ijepes

Distributed plug-and-play optimal generator and load control for power system frequency regulation

Changhong Zhao[a,*], Enrique Mallada[b], Steven H. Low[c], Janusz Bialek[d]

[a] National Renewable Energy Laboratory, Golden, CO 80401, USA
[b] Department of Electrical and Computer Engineering, Johns Hopkins University, Baltimore, MD 21218, USA
[c] Department of Electrical Engineering, California Institute of Technology, Pasadena, CA 91125, USA
[d] Center for Energy Systems, Skolkovo Institute of Science and Technology, Moscow 143026, Russia

ARTICLE INFO

Keywords:
Frequency regulation
Distributed control

ABSTRACT

A distributed control scheme, which can be implemented on generators and controllable loads in a plug-and-play manner, is proposed for power system frequency regulation. The proposed scheme is based on local measurements, local computation, and neighborhood information exchanges over a communication network with an arbitrary (but connected) topology. In the event of a sudden change in generation or load, the proposed scheme can restore the nominal frequency and the reference inter-area power flows, while minimizing the total cost of control for participating generators and loads. Power network stability under the proposed control is proved with a relatively realistic model which includes nonlinear power flow and a generic (potentially nonlinear or high-order) turbine-governor model, and further with first- and second-order turbine-governor models as special cases. In simulations, the proposed control scheme shows a comparable performance to the existing automatic generation control (AGC) when implemented only on the generator side, and demonstrates better dynamic characteristics than AGC when each scheme is implemented on both generators and controllable loads. Simulation results also show robustness of the proposed scheme to communication link failure.

1. Introduction

Maintaining power system frequency tightly around its nominal value, e.g., 60 Hz in US, is critical for satisfactory performance of electrical loads, safety of generating equipment, and reliable power delivery [1]. Off-nominal frequency caused by imbalance between power supply and demand is traditionally corrected through primary and secondary frequency control of generators. Primary frequency control stabilizes frequency to a point that may still be off-nominal via decentralized droop response of speed governors [2]. Secondary frequency control, traditionally known as automatic generation control (AGC) [2,3], adjusts generator setpoints in each control area via centralized integral or proportional-integral control, to restore the nominal frequency and the reference inter-area power flows. This work focuses on secondary frequency control and refers to it as frequency regulation [4].[1]

As larger variations in power imbalance arise from the deepening penetration of intermittent renewable generation, AGC may not be adequate to meet the required frequency standards [1,5]. Tackling this challenge requires either increased fast-acting spinning reserves, which incur high operating cost and emissions [5,6], or alternative resources for frequency regulation, such as controllable loads [6–8]. To exploit the full potential of load control, a set of important issues need to be addressed, including: (i) scalability and flexibility of the control system to support autonomous and plug-and-play operations of controllable loads [9]; (ii) coordination between controllable loads, as well as coordination between loads and generators, to ensure a predictable and stable system behavior [7]; (iii) comfort of controllable load users [6,7] optimized jointly with economic efficiency of generators [1]. Addressing these issues calls for the transformation of power systems from a centralized, hierarchical control architecture, which typically features a timescale separation between economic dispatch and AGC, to a distributed, open-access architecture that integrates optimality and stability objectives [9,10]. Towards this transformation, recent endeavors [9,11–24] are dedicated to developing distributed control algorithms, which can stabilize a power network at an equilibrium that solves an appropriate optimization problem and meets the frequency regulation requirements.

It is common for these studies to use simplified power network models to facilitate controller design and stability analysis. For

* Corresponding author.
E-mail addresses: changhong.zhao@nrel.gov (C. Zhao), mallada@jhu.edu (E. Mallada), slow@caltech.edu (S.H. Low), j.bialek@skoltech.ru (J. Bialek).

[1] In some other literature, frequency regulation includes both primary and secondary frequency control.

https://doi.org/10.1016/j.ijepes.2018.03.014
Received 20 September 2017; Received in revised form 12 January 2018; Accepted 10 March 2018

example, [11–18] consider linearized power flow; [21] assumes the power network has a tree topology; [9,11–13,18–20] ignore the generator turbine-governor dynamics, and [14–17,21] use a simplified first-order turbine-governor model. Compared to [9,11,13–21], a more realistic power network model, which includes a nonlinear power flow model and a second-order turbine-governor model, is used in [22–24]. Moreover, stability conditions for a generic (potentially higher-order or nonlinear) turbine-governor model are obtained in [22] with a passivity-based method.

This paper proposes a distributed optimal generator and load control scheme for frequency regulation. In case of imbalance between power supply and demand, the proposed scheme can restore the nominal frequency and the reference inter-area power flows, while minimizing the total cost of control for participating generators and loads. In the proposed scheme, every control agent for a generator or controllable load measures its local frequency and power flows, performs moderate computations, and communicates with its neighboring agents in a communication network with an arbitrary topology (as long as it connects all the agents). Such a distributed scheme is suitable for autonomous and plug-and-play operations. For example, an agent can plug-in and participate in frequency regulation after updating its information with its neighboring agents. This significantly reduces the system operator's burden of interacting with a large number of agents: maintaining their information, communicating with them, and performing centralized computations for all of them. Such a distributed and plug-and-play scheme can also improve robustness of the system against a single-point failure of the communication or computation functions.

This work complements the literature in the following aspects:

(i) Stability is established for a nonlinear power flow model and a generic (potentially nonlinear or high-order) turbine-governor model, and further for first- and second-order turbine-governor models as special cases. This extends all the studies above except [22]. Compared to [22], the stability condition in this paper for the generic turbine-governor model features a simpler supply rate function. Moreover, the proposed control fulfills the inter-area flow requirement, which was ignored in [22].
(ii) By utilizing and extending the concept of virtual flow in [13], we develop a controller with simpler and more flexible communication than [13,24] and a less restrictive stability condition than [24]; see the discussion in Section 4.
(iii) Simulation results on Power System Toolbox [25] show that the proposed control achieves a comparable performance to AGC when implemented purely on the generator side. Moreover, the proposed control demonstrates better dynamic characteristics than AGC when each scheme is implemented on both generators and controllable loads. Robustness of the proposed control to communication link failure is also observed in simulations.

The rest of this paper is organized as follows. Section 2 introduces the power network model. Section 3 formulates an optimization problem which encapsulates the goals of frequency regulation. Section 4 proposes a distributed frequency regulation scheme. Section 5 proves that the proposed scheme can stabilize the power network at an equilibrium that solves the formulated optimization, and thus restores the nominal frequency and the reference inter-area flows while minimizing the total cost of control. Section 6 shows the simulation results. Finally, Section 7 concludes the paper.

2. System setup

2.1. Notation

Number, vector, and matrix: Let $\mathbb{R}$ denote the set of real numbers and $\mathbb{N}$ the set of natural numbers. For a finite set $S \subset \mathbb{N}$, let $|S|$ denote its cardinality. For a set of scalar numbers $\{a_i \,|i \in S\}$, let a_S denote the column vector of the a_i's; the subscript S is dropped when it is clear from the context. The stacked column vector of two vectors $a \in \mathbb{R}^{|S|}$ and $a' \in \mathbb{R}^{|S'|}$ is denoted by (a,a'). Given any matrix A, denote its transpose by A^T, and its i-th row by A_i. Let A_S denote the submatrix of A composed only of the rows A_i for $i \in S$. The diagonal matrix with diagonal entries $\{a_i \,|i \in S\}$ is denoted interchangeably by $\mathrm{diag}(a_i, i \in S)$, $\mathrm{diag}(a_S)$, and a_S (when it can be distinguished from the vector a_S by the context). Let $\mathbf{1}_S$ ($\mathbf{0}_S$) denote the $|S|$-dimensional column vector of all ones (zeros), which is often simplified as 1 (0) when its dimension is obvious from the context.

Power network: Consider a power transmission network represented by a *directed*, connected graph $(\mathcal{N},\mathcal{E})$, where $\mathcal{N}$ is the set of buses, and $\mathcal{E}$ is the set of transmission lines. A transmission line indexed the e-th in $\mathcal{E}$ and directed from buses i to j is denoted interchangeably by $e \in \mathcal{E}$ and $ij \in \mathcal{E}$. The symbol $i \sim j$ means either $ij \in \mathcal{E}$ or $ji \in \mathcal{E}$ without distinguishing the direction of the link. The set $\mathcal{N}$ of buses is partitioned as $\mathcal{N} = \mathcal{G} \cup \mathcal{L}$ where $\mathcal{G}$ and $\mathcal{L}$ are the sets of generator and load buses, respectively. A generator bus connects to a generator with large inertia. A load bus represents the aggregate of a substation and the distributed energy resources and loads connected to it. The power network $(\mathcal{N},\mathcal{E})$ is divided into a set $\mathcal{K}$ of subgraphs, called control areas.

Communication network: Each bus $i \in \mathcal{N}$ has an agent which decides its local control actions by measuring local frequency and power flows, performing moderate computations, and communicating with its neighboring agents in an *undirected* (two-way), connected graph $(\mathcal{N},\mathcal{E}')$. The topology of the communication network $(\mathcal{N},\mathcal{E}')$ can be arbitrary, and in particular can be different from the power network $(\mathcal{N},\mathcal{E})$, as long as it connects all the buses in $\mathcal{N}$. Notations $ij \in \mathcal{E}'$ and $i \leftrightarrow j$ are used interchangeably to indicate that the agents at buses i and j communicate with each other. A positive constant weight $B'_{ij} = B'_{ji}$ is assigned to every communication link $ij \in \mathcal{E}'$. The choice of B'_{ij} is also arbitrary; see a further comment in Section 4. Although the proposed controller in Section 4 and its optimality and stability analysis in Section 5 assume that every bus has a control agent that can compute and communicate, in the simulations in Section 6 the control agents are only installed at a subset of buses which have controllable generators and loads.

Other frequently used notations are listed below:

	Variables
θ_i, $i \in \mathcal{N}$	bus voltage phase angles
ω_i, $i \in \mathcal{N}$	*deviations* of bus frequencies from the nominal value
r_i, $i \in \mathcal{N}$	frequency-insensitive uncontrollable power injections
p_i^{m}, $i \in \mathcal{G}$	mechanical power outputs of generators
p_i, $i \in \mathcal{G}$	generation control commands
d_i, $i \in \mathcal{N}$	real power consumption of controllable loads
P_{ij}, $ij \in \mathcal{E}$	transmission line power flows. Define $P_{ji} := -P_{ij}$
	Constants
M_i, $i \in \mathcal{G}$	positive generator inertia constants
D_i, $i \in \mathcal{N}$	positive load-damping constants
B_{ij}, $ij \in \mathcal{E}$	positive constant line parameters. Define $B_{ji} := B_{ij}$
C_{ie}, $i \in \mathcal{N}$, $e \in \mathcal{E}$	$C_{ie} = 1$ if $e = ij$ for some bus j, $C_{ie} = -1$ if $e = \ell i$ for some bus ℓ, and $C_{ie} = 0$ otherwise. $C \in \mathbb{R}^{\lvert\mathcal{N}\rvert \times \lvert\mathcal{E}\rvert}$ is the incidence matrix of $(\mathcal{N},\mathcal{E})$
E_{ki}, $k \in \mathcal{K}$, $i \in \mathcal{N}$	$E_{ki} = 1$ if bus i is in control area k, and $E_{ki} = 0$ otherwise

2.2. Power network model

Consider the standard power network model [2,3]:

$$\dot{\theta}_i = \omega_i\,, \quad \forall\, i \in \mathcal{N} \tag{1a}$$

$$M_i\dot{\omega}_i = r_i + p_i^{\mathrm{m}} - d_i - D_i\omega_i - \sum_{j:i\sim j} P_{ij}\,, \quad \forall\, i \in \mathcal{G} \tag{1b}$$

$$0 = r_i - d_i - D_i\omega_i - \sum_{j:i\sim j} P_{ij}\,, \quad \forall\, i \in \mathcal{L} \tag{1c}$$

$$P_{ij} = B_{ij}\sin(\theta_i - \theta_j)\,, \quad \forall\, ij \in \mathcal{E}. \tag{1d}$$

In (1a), θ_i is the bus i voltage phase angle relative to a rotating frame of the nominal frequency, and ω_i is the deviation of bus i frequency from the nominal value.Equation (1b) is the inertial and load-frequency dynamics associated with bulk generators, and (1c) presents the power balance at load buses. The r_i in (1b) and (1c) denotes the frequency-insensitive, uncontrollable net real-power injection to bus i. A change in r_i may arise from, e.g., a change in non-dispatchable renewable generation, a change in load, or loss of a generator. In particular, by modeling changes in renewable generation as r_i, we assume that the renewable energy sources do not provide frequency response, and that their internal dynamics are fast enough to be neglected for the time-scale of frequency regulation. These assumptions were made in, e.g., [1]. Also, the proposed control will deal with the variability and uncertainty of renewable generation in a real-time feedback fashion, and hence the model (1) assumes the realizations of renewable generation to be available and captured by r_i. Every bus $i \in \mathcal{N}$ has an aggregate controllable load whose real-power consumption is d_i and an aggregate frequency-sensitive, uncontrollable load, like a group of induction motors, whose real-power consumption changes by $D_i\omega_i$ with frequency deviation ω_i. At any given instant of time, all the loads (controllable, uncontrollable frequency-sensitive and insensitive) in (1b) and (1c) are treated as constant-real-power loads. Controller design and analysis with other load models, e.g., constant-current and constant-impedance, will be the subject of future research. In Section 6, we simulate a network that contains constant-power, constant-current, and constant-impedance loads to test the proposed controllers. The power flow P_{ij} is modeled by (1d), where with the positive constant B_{ij} it is assumed that the lines are purely inductive and the bus voltage magnitudes are fixed. Let C be the incidence matrix of the power network $(\mathcal{N},\mathcal{E})$, and define $\theta_{ij} := \theta_i - \theta_j$, so that $C^T\theta = (\theta_{ij}, ij \in \mathcal{E})$ collects the phase angle differences across all the lines. In practical power networks, besides generator buses in $\mathcal{G}$ modeled in (1b) and load buses in $\mathcal{L}$ modeled in (1c), there are also buses with neither a generator nor a load, for which the power balance equation reads $\sum_{j:i\sim j} P_{ij} = 0$. Model (1) has eliminated this kind of buses through Kron reduction [26], without influencing the power injections and power balance at generator and load buses. It will be future work to consider a full network model without such reduction.

Each generator bus $i \in \mathcal{G}$ has an aggregate generator whose mechanical power output is p_i^{m}. A generation control command p_i drives p_i^{m} through the following turbine-governor dynamics:

$$(\dot{p}_i^{\mathrm{m}}, \dot{a}_i) = g_i(p_i^{\mathrm{m}}, a_i, p_i - \omega_i/R_i)\,, \quad \forall\, i \in \mathcal{G} \tag{2}$$

where a_i denotes an internal state vector, and R_i is a constant coefficient for the standard droop frequency control.

Assumption 1. Given any $p_i \in \mathbb{R}$, there exists a unique point (p_i^{m}, a_i) such that $g_i(p_i^{\mathrm{m}}, a_i, p_i) = 0$. Moreover, $p_i^{\mathrm{m}} = p_i$ at this point.

Assumption 1 means that the generator internal state and mechanical power are uniquely determined by the control command, and the mechanical power equals the control command, at any steady state where the frequency is nominal. A classic example of (2), which satisfies Assumption 1, is the following second-order model [3]:

$$T_{\mathrm{g},i}\dot{a}_i = -a_i + p_i - \omega_i/R_i\,, \quad \forall\, i \in \mathcal{G} \tag{3a}$$

$$T_{\mathrm{t},i}\dot{p}_i^{\mathrm{m}} = -p_i^{\mathrm{m}} + a_i\,, \quad \forall\, i \in \mathcal{G} \tag{3b}$$

where a_i is the valve position, and the time constants $T_{\mathrm{g},i}$ and $T_{\mathrm{t},i}$ characterize the time for governor and turbine to fully respond to a change in their input. Given the fact that $T_{\mathrm{g},i}$ is usually much smaller than $T_{\mathrm{t},i}$, the model (3) can be simplified as the following first-order model [15,21–23]:

$$T_{\mathrm{t},i}\dot{p}_i^{\mathrm{m}} = -p_i^{\mathrm{m}} + p_i - \omega_i/R_i\,, \quad \forall\, i \in \mathcal{G} \tag{4}$$

which also satisfies Assumption 1. The internal state vector a_i in (2) is allowed to be zero-dimensional to accommodate a special case like (4) which indeed has no internal state.

Loads can respond much faster than generators to changes in their input [6,27], and hence the model (1) ignores the dynamics of loads. For simulations in Section 6, the first-order lag dynamics of loads in [16] is modeled.

3. Problem formulation

An *equilibrium* of (1)–(2) is defined as a solution of (1)–(2) where all the time derivatives $(\dot{\theta},\dot{\omega}_{\mathcal{G}},\dot{p}_{\mathcal{G}}^{\mathrm{m}},\dot{a}_{\mathcal{G}}) = 0$. By (1a), an equilibrium requires $\omega = 0$, i.e., all the bus frequencies to be nominal. Suppose that the system (1)–(2) initially operates at an equilibrium where the inter-area power flows are considered to be the reference. At a certain time, step changes in uncontrollable power injections r_i occur at an arbitrary subset of $\mathcal{N}$, causing the system state, particularly bus frequencies and power flows, to deviate from the equilibrium. It then relies on frequency regulation to restore the nominal frequency and the reference inter-area power flows. We now formulate the goals of frequency regulation as an optimization problem.

Given $r \in \mathbb{R}^{|\mathcal{N}|}$ after the aforementioned step change, frequency regulation aims at stabilizing the system (1)–(2) to an equilibrium that solves the optimization problem below. Following the convention in our earlier work [12,13], this problem is called *optimal load control (OLC)*, though it incorporates both generator and load control.

OLC:

$$\min_{\substack{\underline{p}_{\mathcal{G}} \leqslant p_{\mathcal{G}} \leqslant \overline{p}_{\mathcal{G}} \\ \underline{d} \leqslant d \leqslant \overline{d}, P}} \quad \sum_{i\in\mathcal{G}} c_i^p(p_i) + \sum_{i\in\mathcal{N}} c_i^d(d_i) \tag{5a}$$

$$\text{subject to} \quad r_i + p_i = d_i + \sum_{j:i\sim j} P_{ij}\,, \quad \forall\, i \in \mathcal{N} \tag{5b}$$

$$\sum_{i\in\mathcal{N}} E_{ki} \sum_{j:i\sim j} P_{ij} = \widehat{P}_k\,, \quad \forall\, k \in \mathcal{K}. \tag{5c}$$

In (5a), the constants $\underline{p}_i \leqslant \overline{p}_i$ for $i \in \mathcal{G}$ and $\underline{d}_i \leqslant \overline{d}_i$ for $i \in \mathcal{N}$ specify the feasible regions, or control capacity limits, of generators and controllable loads. The case where there is no controllable generator or load at bus i can be handled by setting $\underline{p}_i = \overline{p}_i = 0$ or $\underline{d}_i = \overline{d}_i = 0$. Functions c_i^p for $i \in \mathcal{G}$ quantify the cost of generator control due to, e.g., loss of economic efficiency caused by deviation from the reference generation, and c_i^d for $i \in \mathcal{N}$, which are the cost (or disutility) functions for load control, quantify the discomfort of controllable load users due to deviation from their preferred/reference power usage [11,21,22]. Note that the model (1) considers aggregates of loads at the transmission level. Therefore a disutility function c_i^d maps the aggregate power deviation to the aggregate discomfort of a group of devices, and does not necessarily reflect each individual thermostat temperature deviation or pool pump degradation, et cetera. Modeling discomfort of individual devices, although important, is out of the scope of this proof-of-concept work. The constraint (5b) imposes power balance at each bus $i \in \mathcal{N}$, [2] which ensures restoration of the nominal frequency. The constraint (5c) enforces the standard inter-area flow requirement, i.e., the net power flows out of areas $k \in \mathcal{K}$ must equal their reference values $\widehat{P}_k$.

[2] Define constants $p_i = p_i^* = p_i^{\mathrm{m}} = p_i^{\mathrm{m},*} = M_i \equiv 0$ for all $i \in \mathcal{L}$.

Assumption 2. The cost functions c_i^p for $i \in \mathscr{G}$ and c_i^d for $i \in \mathscr{N}$ are strictly convex and twice continuously differentiable on $[\underline{p}_i, \overline{p}_i]$ and $[\underline{d}_i, \overline{d}_i]$ respectively.

Assumption 3. There exists $(C^T\theta^*, p_{\mathscr{G}}^*, d^*, P^*)$ which satisfies: (i) $(p_{\mathscr{G}}^*, d^*, P^*)$ is optimal for OLC (5); and (ii) $P_{ij}^* = B_{ij}\sin(\theta_{ij}^*)$ and $|\theta_{ij}^*| < \pi/2$ for all $ij \in \mathscr{E}$.

The region where $|\theta_{ij}^*| < \pi/2$ for all $ij \in \mathscr{E}$ is called the *principal region*, in which a power-flow solution is stable [28]. The existence of a solution as described in Assumption 3, together with Assumption 2, leads to the uniqueness of such a solution, as shown by the following lemma.

Lemma 1. *Suppose Assumptions 2 and 3 hold. Then there exists a unique* $(C^T\theta^*, p_{\mathscr{G}}^*, d^*, P^*)$ *which satisfies: (i)* $(p_{\mathscr{G}}^*, d^*, P^*)$ *is optimal for OLC (5); and (ii)* $P_{ij}^* = B_{ij}\sin(\theta_{ij}^*)$ *and* $|\theta_{ij}^*| < \pi/2$ *for all* $ij \in \mathscr{E}$.

Proof. Such a $(C^T\theta^*, p_{\mathscr{G}}^*, d^*, P^*)$ exists by Assumption 3, where $(p_{\mathscr{G}}^*, d^*)$ is unique by strict convexity of c_i^p and c_i^d. Given $(p_{\mathscr{G}}^*, d^*)$, the equations

$$r_i + p_i^* = d_i^* + \sum_{j:i\sim j} B_{ij}\sin(\theta_{ij}^*), \quad \forall\, i \in \mathscr{N} \tag{6}$$

admit a unique solution $C^T\theta^*$ in the region where $|\theta_{ij}^*| < \pi/2$ for all $ij \in \mathscr{E}$ [28]. This implies the uniqueness of P^*. □

4. Controller design

The following controller (7), which determines the generator and load controls (p,d), is proposed to achieve the goals formalized in OLC (5). The derivation of controller (7) is inspired by [13,24] which computed cyber signals called virtual flows to estimate the actual power flows. However, controller (7) differs from and improves upon those in [13,24] as discussed at the end of this section.

$$p_i = p_i(\lambda_i,\omega_i) := [(c_i^p)'^{-1}(-\lambda_i+\omega_i)]_{\underline{p}_i}^{\overline{p}_i} + \omega_i/R_i \tag{7a}$$

$$d_i = d_i(\lambda_i,\omega_i) := [(c_i^d)'^{-1}(\lambda_i+\omega_i)]_{\underline{d}_i}^{\overline{d}_i} \tag{7b}$$

$$\dot{\lambda}_i = K_i^{\lambda}\left(M_i\dot{\omega}_i + D_i\omega_i + \sum_{j:i\sim j} P_{ij} - \sum_{j:i\leftrightarrow j} B'_{ij}(\phi_i-\phi_j)\right) \tag{7c}$$

$$\dot{\phi}_i = \lambda_i - \sum_{k\in\mathscr{K}} E_{ki}\pi_k \tag{7d}$$

$$\dot{\pi}_k = K_k^{\pi}\left(\sum_{i\in\mathscr{N}} E_{ki}\sum_{j:i\leftrightarrow j} B'_{ij}(\phi_i-\phi_j) - \widehat{P}_k\right) \tag{7e}$$

where (7a) is for all the generator buses $i \in \mathscr{G}$, (7b)–(7d) are for all the buses $i \in \mathscr{N}$, and (7e) is for all the control areas $k \in \mathscr{K}$. Recall that $i \leftrightarrow j$ denotes a two-way communication link between the control agents at buses i and j. The topology of the communication network can be arbitrary, as long as it connects all the buses in $\mathscr{N}$. The positive constant weights B'_{ij} on communication links and the positive constant gains K_i^{λ} and K_k^{π} can also be arbitrarily selected. These choices will not affect the system equilibrium and stability (if feedback delays are negligible), as shown in Section 5. However, they may have significant impacts on the dynamic performance of the system, including frequency nadir, rate of convergence, and magnitudes of oscillations. Such impacts need future investigation.

Define the following function:

$$[(f)'^{-1}(x)]_a^b := \begin{cases} a, & x \in (-\infty, f'(a)] \\ (f)'^{-1}(x), & x \in (f'(a), f'(b)] \\ b, & x \in (f'(b), +\infty) \end{cases}$$

with which the functions $p_i(\cdot,\cdot)$ and $d_i(\cdot,\cdot)$ in (7a) and (7b) are well defined by Assumption 2. The $+\,\omega_i/R_i$ term in (7a) cancels the droop control signal $-\omega_i/R_i$ in (2), (3a), and (4), as inspired by [16,17]. Indeed, the function $(c_i^p)'^{-1}(\cdot)$, with ω_i in its input, effectively encapsulates primary frequency control. While the frequency deviation ω_i can be measured locally at bus i, the other input λ_i to (7a) and (7b) is a cyber signal calculated in a distributed way by (7c)–(7e).

In (7c), every bus $i \in \mathscr{N}$ calculates λ_i from the local frequency deviation ω_i, power flows P_{ij} to neighboring buses j in the power network, a local cyber signal ϕ_i, and signals ϕ_j received from neighboring buses j in the communication network. Since λ_i is the integral of the right-hand-side of (7c), calculating λ_i needs a proportional term of ω_i with the coefficient M_i and an integral term of ω_i with the coefficient D_i, thus avoiding taking the derivative of ω_i which may introduce intense noise. The cyber signal ϕ_i is calculated by (7d), where $\sum_{k\in\mathscr{K}} E_{ki}\pi_k$ equals $\pi_{k'(i)}$ if bus i is in area $k'(i)$. For each area k, a signal π_k is calculated by (7e) and broadcast to all the buses in area k such that they can execute (7d). In (7e), every control area k indeed only sums $B'_{ij}(\phi_i-\phi_j)$ over $i \leftrightarrow j$ where i is in area k and j is in another area.

Discussion:

(i) The design of (7) borrows the idea of virtual phase angles ϕ_i and virtual flows $B'_{ij}(\phi_i-\phi_j)$ from [13]. The computation of ϕ in [13], based on a primal-dual algorithm for OLC, requires communication of λ and π between adjacent buses and areas. Different from [13], in designing (7) we interpret λ_i as the virtual frequency deviation, by noticing the similarity between (7c) and (1b). Based on this interpretation, a simpler computation (7d) for ϕ_i is proposed, where a bus i in area $k'(i)$ only needs the local virtual frequency deviation λ_i and an intra-area broadcast signal $\pi_{k'(i)}$.

(ii) In [13] both the actual power flow $P_{ij} = B_{ij}(\theta_i-\theta_j)$ and the virtual flow $B_{ij}(\phi_i-\phi_j)$ are linear. In [24], a nonlinear virtual flow $B_{ij}\sin(\phi_i-\phi_j)$ was designed to emulate the nonlinear power flow $P_{ij} = B_{ij}\sin(\theta_i-\theta_j)$. Here in (7), the *linear virtual* flow is used under the nonlinear power flow model, which makes the equilibrium ϕ^* unique modulo a rigid shift (see Section 5), and relaxes the stability condition in [24] which restricted ϕ^* to the principal region.

(iii) Compared to [13,24], the proposed control (7) is more flexible, by allowing the topology of the communication network to be arbitrary (as long as it connects all the buses) and possibly different from the power network, and the control parameters B'_{ij} to be arbitrary and possibly different from the physical parameters B_{ij}. With such flexibility, the equilibrium virtual flow may no longer equal the equilibrium power flow on every power line or communication link (they are equal in [13]). However, the total equilibrium virtual flow incident to bus i, i.e., $\sum_{j:i\leftrightarrow j} B'_{ij}(\phi_i^*-\phi_j^*)$, can still precisely estimate the equilibrium net power injection at bus i, as shown later in (14). This relationship lays a foundation for the proposed controller (7) to eliminate power imbalance and restore the nominal frequency at every bus, as will become clear in Section 5.

(iv) The proposed scheme (7) assumes that all the buses perform measurement, computation, and communication, though not all of them are controllable (recall that we set $\underline{p}_i = \overline{p}_i = 0$ and $\underline{d}_i = \overline{d}_i = 0$ for uncontrollable generators and loads, which makes their control actions constantly zero by (7a) and (7b)). It is our future work to develop control schemes under a sparse placement of control agents and a sparse communication network, which do not cover all the transmission buses. Moreover, (7) is given in continuous time, whereas in practice the measurement and communication are carried out in discrete time, asynchronously, and even on a low time resolution, especially when the existing supervisory control and data acquisition (SCADA) system is used. This in general may negatively impact system stability, which calls for further investigation to understand. As a preliminary study, Section 6 will show simulation results under sparse computation, communication, and control, as well as a discrete-time implementation.

5. Performance analysis

This section analyzes the equilibrium and stability of the closed-loop system (1), (2), (7) under the proposed control. Section 5.1 shows that the system has an optimal equilibrium that solves OLC (5) and therefore restores the nominal frequency and the reference inter-area flows while minimizing the total cost of control. Section 5.2 proves convergence of the system to this optimal equilibrium under certain conditions. Results in Sections 5.1 and 5.2 are then applied to the second-order (3) and first-order (4) turbine-governor models, which are special cases of the generic turbine-governor model (2).

5.1. Equilibrium analysis

Let C' be the incidence matrix of the communication network $(\mathscr{N},\mathscr{E}')$ by assigning an arbitrary direction to each undirected link $e' \in \mathscr{E}'$. Moreover, we arbitrarily construct a directed graph $(\mathscr{K},\mathscr{E}'')$ that connects all the control areas $k \in \mathscr{K}$, and let C'' be the incidence matrix of $(\mathscr{K},\mathscr{E}'')$. The following notations are defined for ease of exposition.

Definition 1. For the closed-loop system (1), (2), (7):

(i) $x \coloneqq (C^T\theta,\omega,P,p_{\mathscr{G}}^{\mathrm{m}},a_{\mathscr{G}})$ is the vector of physical states, $u \coloneqq (p_{\mathscr{G}},d)$ is the vector of control inputs, and $z \coloneqq (\lambda,\pi,C'^T\phi)$ is the vector of cyber signals.
(ii) An *equilibrium* is a solution (x^*,u^*,z^*) of the closed-loop system (1), (2), (7) which makes $(\dot\theta,\dot\omega_{\mathscr{G}},\dot p_{\mathscr{G}}^{\mathrm{m}},\dot a_{\mathscr{G}},\dot\lambda,\dot\pi) = 0$ and $\dot\phi_i = \dot\phi_j$ for all $i,j \in \mathscr{N}$.
(iii) Y_Θ^* is the set of all the equilibria (x^*,u^*,z^*) that satisfy $|\theta_{ij}^*| < \pi/2$ for all $ij \in \mathscr{E}$.
(iv) Every point $(x^*,u^*,z^*) \in Y_\Theta^*$ is an *optimal equilibrium*.

As shown in Definition 1(i), we care about the differences $C^T\theta$ between actual phase angles across power lines, and the differences $C'^T\phi$ between virtual phase angles across communication links. In equilibrium, the vector θ must be fixed, while a rigid rotation of ϕ is allowed, as shown by (ii). The equilibrium set Y_Θ^* defined in (iii) is restricted to the principal region of phase angles. The following theorem reveals important properties of Y_Θ^*, and in particular explains why all the equilibria in Y_Θ^* are defined to be optimal in (iv).

Theorem 1. *Suppose Assumptions 1–3 hold. Then the system (1), (2), (7) has a nonempty equilibrium set Y_Θ^* where (x^*,u^*) is unique and $(p_{\mathscr{G}}^*,d^*,P^*)$ is optimal for OLC (5).*

See Appendix A.1 for the proof of Theorem 1. While Theorem 1 points out the uniqueness of (x^*,u^*) over all the optimal equilibria, the following theorem reveals the structure of $z^* = (\lambda^*,\pi^*,C'^T\phi^*)$ in equilibrium.

Theorem 2. Suppose Assumptions 1–3 hold. Then all the equilibria (x^*,u^*,z^*) of (1), (2), (7) satisfy the following:

(i) $C'^T\phi^*$ is unique.
(ii) $\lambda_i^* = \lambda_j^*$ for all the buses i,j in the same control area.
(iii) Suppose that an area k contains a bus j such that $\underline{p}_j < p_j^* < \overline{p}_j$ (if $j \in \mathscr{G}$) or $\underline{d}_j < d_j^* < \overline{d}_j$. Then $\lambda_{\mathscr{N}(k)}^*$, where $\mathscr{N}(k)$ denotes the set of all the buses in area k, is unique.
(iv) Suppose that every area $k \in \mathscr{K}$ contains a bus $j(k)$ such that $\underline{p}_{j(k)} < p_{j(k)}^* < \overline{p}_{j(k)}$ (if $j(k) \in \mathscr{G}$) or $\underline{d}_{j(k)} < d_{j(k)}^* < \overline{d}_{j(k)}$. Then $(\lambda^*,C'^T\pi^*)$ is unique.

Proof. (i) $C'^T\phi^*$ is unique by (14) and the uniqueness of $(p_{\mathscr{G}}^{\mathrm{m},*} = p_{\mathscr{G}}^*,d^*)$; (ii) results from (7d) and the definition of equilibrium where $\dot\phi_i = \dot\phi_j$ for all $i,j \in \mathscr{N}$; (iii) results from (ii), (7a) and (7b), the uniqueness of $(p_{\mathscr{G}}^*,d^*)$, and the fact that $\omega^* = 0$; in (iv), the uniqueness of λ^* is straightforward from (iii), and the uniqueness of $C'^T\pi^*$ results from the uniqueness of λ^* and (7d). □

Note that Theorem 2 holds for all the equilibria of (1), (2), (7), not only those optimal equilibria in Y_Θ^*. Theorem 2 shows that, under certain conditions, the equilibrium (λ^*,π^*,ϕ^*) is unique, modulo rigid shifts of π^* and ϕ^*. In particular, λ^* is unique if each control area has at least one controllable generator or load that does not reach its control capacity limit.

5.2. Stability analysis

The following assumption serves as the main stability condition for the optimal equilibrium set Y_Θ^*.

Assumption 4. Let (x^*,u^*) be the unique subvector over Y_Θ^*, [3] and define $(\widetilde{x},\widetilde{u}) \coloneqq (x,u)-(x^*,u^*)$. For each generator bus $i \in \mathscr{G}$, there exists a function $U_i(\widetilde{p}_i^{\mathrm{m}},\widetilde{a}_i)$ which satisfies: (i) $U_i(\widetilde{p}_i^{\mathrm{m}},\widetilde{a}_i) \geqslant 0$; (ii) $U_i(\widetilde{p}_i^{\mathrm{m}},\widetilde{a}_i) = 0$ if and only if $(\widetilde{p}_i^{\mathrm{m}},\widetilde{a}_i) = 0$; and (iii) U_i is radially unbounded, i.e., $|U_i(\widetilde{p}_i^{\mathrm{m}},\widetilde{a}_i)| \to +\infty$ if $\|(\widetilde{p}_i^{\mathrm{m}},\widetilde{a}_i)\|_2 \to +\infty$. Moreover, let $\dot U_i \coloneqq [\partial U_i/\partial(\widetilde{p}_i^{\mathrm{m}},\widetilde{a}_i)]g_i$ be the time derivative of U_i along the trajectory of (2). Then

$$h_i \coloneqq \dot U_i + (\widetilde{p}_i^{\mathrm{m}}-\widetilde{d}_i)(\widetilde{\lambda}_i + \widetilde{\omega}_i) \leqslant 0\,, \quad \forall\, i \in \mathscr{G}, \tag{8}$$

and $h_i = 0$ if and only if $(\widetilde{d}_i,\widetilde{p}_i^{\mathrm{m}},\widetilde{a}_i) = 0$.

Each generator bus $i \in \mathscr{G}$ can be interpreted as a subsystem, whose input is $(-\widetilde{\lambda}_i-\widetilde{\omega}_i)$, i.e., the input to the generator and load control functions (7a) and (7b), and whose output is $(\widetilde{p}_i^{\mathrm{m}}-\widetilde{d}_i)$, i.e., the net power injection to the network. Then Assumption 4 essentially indicates passivity of these subsystems [29, Definition 6.3]. Such passivity-based methods have been applied to stability analysis of primary frequency control [30], secondary frequency control [22,23], coupled frequency-voltage-market dynamics [20], and distributed control systems with communication delays [31]. Compared to [22], the supply rate function in Assumption 4, i.e., $(\widetilde{p}_i^{\mathrm{m}}-\widetilde{d}_i)(\widetilde{\lambda}_i + \widetilde{\omega}_i)$, is much simpler. Compared to [23] which focuses on the second-order (3) and first-order (4) turbine-governor models, Assumption 4 is made for the generic model (2) which can potentially be of a higher order or nonlinear, and thus more realistic. For classic examples of turbine-governor models such as (3) and (4), quadratic functions U_i satisfying Assumption 4 can be found explicitly under moderate technical conditions, as shown later in Theorems 4 and 5 and their proofs in Appendices A.3 and A.4.

Theorem 3. *Suppose Assumptions 1–4 hold. Then the system (1), (2), (7) has a nonempty equilibrium set Y_Θ^* where (x^*,u^*) is unique and $(p_{\mathscr{G}}^*,d^*,P^*)$ is optimal for OLC (5). Moreover, $(x(t),u(t)) \to (x^*,u^*)$ as $t \to +\infty$, for every trajectory $(x(t),u(t),z(t))$ of (1), (2), (7) that starts close enough to Y_Θ^*.*

See Appendix A.2 for the proof of Theorem 3. This theorem indicates the convergence of physical states and control inputs to the optimal equilibrium, which means that the proposed control (7) can restore the nominal frequency and the reference inter-area flows in a way that minimizes the total cost of control. The convergence of cyber signals $z(t) = (\lambda(t),\pi(t),C'^T\phi(t))$, albeit not guaranteed by Theorem 3, can be implied under certain circumstances. For instance, if a bus i satisfies either $\underline{p}_i < p_i^* < \overline{p}_i$ or $\underline{d}_i < d_i^* < \overline{d}_i$, then $\lambda_i(t)$ converges to its unique equilibrium λ_i^* as $t \to \infty$, by (7a) and (7b) and the convergence of $(p_{\mathscr{G}}(t),d(t))$.

5.3. Results for specific turbine-governor models

Theorems 4 and 5 below are obtained by applying Theorems 1 and 3 to the second-order (3) and first-order (4) turbine-governor models as special cases of (2). Their proofs are deferred to Appendices A.3 and

[3] Assumptions 1–3 are prerequisites of Assumption 4, such that Y_Θ^* has a unique subvector (x^*,u^*) wherein $(p_{\mathscr{G}}^*,d^*,P^*)$ is optimal for OLC (5), by Theorem 1.

A.4, respectively.

Theorem 4. *Suppose Assumptions 2 and 3 hold. Then the system (1),(3), (7) has a nonempty equilibrium set Y_Θ^* where (x^*,u^*) is unique and $(p_{\mathscr{G}}^*,d^*,P^*)$ is optimal for OLC (5). Moreover, suppose that in a neighborhood of Y_Θ^*, for every $i \in \mathscr{G}$, there are constants $\underline{\beta}_i$ and $\overline{\beta}_i$ which satisfy*[4]:

$$0 \leqslant -\frac{\partial p_i}{\partial \lambda_i}(\lambda_i,\omega_i) < \underline{\beta}_i < \overline{\beta}_i \leqslant \frac{\partial d_i}{\partial \lambda_i}(\lambda_i,\omega_i), \quad \forall\, i \in \mathscr{G}. \tag{9}$$

Then $(x(t),u(t)) \to (x^*,u^*)$ as $t \to +\infty$, for every trajectory $(x(t),u(t),z(t))$ of (1), (3), (7) that starts close enough to Y_Θ^*.

Theorem 5. *Suppose Assumptions 2 and 3 hold. Then the system (1), (4), (7) has a nonempty equilibrium set Y_Θ^* where (x^*,u^*) is unique and $(p_{\mathscr{G}}^*,d^*,P^*)$ is optimal for OLC (5). Moreover, suppose either of the following holds in a neighborhood of Y_Θ^* for every $i \in \mathscr{G}$:*

(i) *there are constants $\underline{\beta}_i$ and $\overline{\beta}_i$ which satisfy:*

$$0 \leqslant -\frac{\partial p_i}{\partial \lambda_i}(\lambda_i,\omega_i) < \underline{\beta}_i < \overline{\beta}_i \leqslant \frac{\partial d_i}{\partial \lambda_i}(\lambda_i,\omega_i), \quad \forall\, i \in \mathscr{G}. \tag{10}$$

(ii) *there is a constant $\beta_i > 0$ which, for all (λ_i,ω_i) in the considered neighborhood of Y_Θ^*, satisfies:*

$$-\frac{\partial p_i}{\partial \lambda_i}(\lambda_i,\omega_i) \equiv \beta_i, \quad \forall\, i \in \mathscr{G}. \tag{11}$$

Then $(x(t),u(t)) \to (x^*,u^*)$ as $t \to +\infty$, for every trajectory $(x(t),u(t),z(t))$ of (1), (4), (7) that starts close enough to Y_Θ^*.

The condition for convergence of $(x(t),u(t))$ in Theorem 4, which is also condition (i) in Theorem 5, is satisfied if every generator bus has a co-located controllable load, whose strength of response (measured by the derivative of p_i or d_i over the input signal λ_i) around the optimal equilibrium is higher than that of the generator. For the first-order turbine-governor model (4), convergence of $(x(t),u(t))$ can also be guaranteed by condition (ii) in Theorem 5, which is satisfied if all the generator control functions (7a) are linear around the optimal equilibrium, i.e., if all the generators have quadratic cost functions and none of them reaches its control capacity limit at the optimal equilibrium. Each of these conditions is sufficient (and likely conservative) for convergence of the corresponding system to (x^*,u^*). Indeed, for the cast of quadratic cost functions (linear control functions), a less conservative stability condition was derived in [22] using the passivity-based method, and we leave it as future work to prove less conservative stability conditions for the general case considered here.

6. Numerical study

To demonstrate performance of the proposed control (7), we simulate the New York-New England 68-bus network in Fig. 1 on Power System Toolbox (PST) [25]. The PST simulation model is more realistic than the model in Section 2.2. Specifically, PST models transient and subtransient reactance of generators, exciters, power system stabilizers, and higher-order turbine-governor dynamics. The first-order lag dynamics of loads [16] is also modeled, with the time constant chosen as 0.5 s [27]. Moreover, PST models the resistance, shunt susceptance, and tap-changing transformers along transmission lines, as well as the dynamics of reactive power and voltage magnitude. To generalize the model (1) where only constant-real-power loads are considered for solving power flow at every time instant, PST simulates the 68-bus network with 50% constant-power, 25% constant-impedance, and 25% constant-current loads. In simulations, both AGC and the proposed control are executed in a discrete-time manner, with the control signals updated every two seconds [6].

6.1. Simulation setup

Parameters of the 68-bus network are obtained from PST. As shown in Fig. 1, this network is divided into five control areas [32]. All the 16 generators, and 18 selected loads, are controllable. A communication graph, which connects these controllable generators and loads in a tree, will be used for the proposed distributed control (7). Although the stability analysis of (7) assumes that all the buses participate in computation and communication, in simulations we only implement (7) on the controllable generators and loads.

The OLC cost functions are $c_i^p(p_i) := (p_i - p_i^{\text{ref}})^2/(2K_i^{\text{OLC}})$ for generators, and $c_i^d(d_i) := (d_i - d_i^{\text{ref}})^2/(2K_i^{\text{OLC}})$ for controllable loads, where p_i^{ref} and d_i^{ref} are the reference generation and load power, respectively, determined by the power flow solution at the beginning of each simulation. These cost functions penalize deviations from the reference generation and load. By (7a) and (7b), the proposed control is $p_i = p_i^{\text{ref}} - K_i^{\text{OLC}}(\lambda_i + \omega_i) + \omega_i/R_i$ and $d_i = d_i^{\text{ref}} + K_i^{\text{OLC}}(\lambda_i + \omega_i)$ for generators and loads, respectively. The droop coefficient R_i of every generator is 5% [2], i.e., a change in frequency by $5\% \times 60 = 3$ Hz leads to a droop control command of 1 per unit (pu) in machine base power. The control gains K_i^{OLC} are selected such that (i) their sum over all the generators and loads equals the sum of $1/R_i$ over all the generators, (ii) they are uniform over all the generators, and over all the controllable loads, respectively, and (iii) they satisfy a specified *percentage of load control*, which is defined as the ratio of the total power adjustment provided by controllable loads to that provided by both loads and generators. For instance, with 50% load control, the ratio between K_i^{OLC} is $\frac{1}{16}:\frac{1}{16}:\ldots:\frac{1}{16}:\frac{1}{18}:\frac{1}{18}\ldots:\frac{1}{18}$ over 16 generators and 18 controllable loads. We will simulate up to 50% load control according to [7,33], which both indicate that the frequency regulation reserve provided by loads can equal or exceed that provided by generators. After a disturbance, the proposed controllers with properly selected K_i^{OLC} will deploy generator- and load-side reserves subject to the specified percentage of load control. To ensure that the specified percentage of load control is precisely imposed, we set large enough control capacities for generators and loads in order not to bind their deployed reserves, i.e., actual power adjustments. Other parameters in (7) are $K_i^\lambda = 2 \times 10^{-3}$ for all the generators and controllable loads, $K_k^\pi = 1 \times 10^{-4}$ for all the control areas, and $B'_{ij} = B'_{ji} = 1 \times 10^6$ for all the communication links.

The traditional frequency regulation scheme, AGC, is simulated as a benchmark. AGC is implemented as in [2, Section 9.7], with the ACE integral gain chosen as 0.08 and the participation factors proportional to K_i^{OLC} in each control area. The ratio between the sums of participation factors over loads and generators determines the percentage of load control.

6.2. Simulation results

At time $t = 1$ s, sudden increases in uncontrollable loads and/or decreases in non-dispatchable renewable generations occur in the system, so that the *net* load makes a step increase of 700 MW at each of Buses 4, 8, 20, 37, 42, and 1400 MW at Bus 52. Imbalance between power supply and demand is introduced to the system in such a way, based on the model of r_i in Section 2.2.

Figs. 2 and 3 show the frequency at Bus 62 (other buses display similar frequency trends) and the deviation of total power flow out of Area 1, respectively, under AGC and the proposed control (7) referred to as OLC, each implemented with 0%, 25%, and 50% load control. It is observed that both AGC and OLC, under different percentages of load control, can successfully restore the frequency to 60 Hz and the inter-area power flow to its reference value. It is also observed from Fig. 2(a) that under zero load control, OLC has a similar dynamic performance, especially frequency nadir, to AGC. Indeed, the control parameters

[4] By (7a) and Assumption 2, $(\partial p_i/\partial \lambda_i)$ exists and is nonpositive for all (λ_i,ω_i) except when $(-\lambda_i - \omega_i)$ equals $(c_i^p)'(\underline{p}_i)$ or $(c_i^p)'(\overline{p}_i)$, in which case $(\partial p_i/\partial \lambda_i)$ represents partial subgradient; similarly for $(\partial d_i/\partial \lambda_i)$.

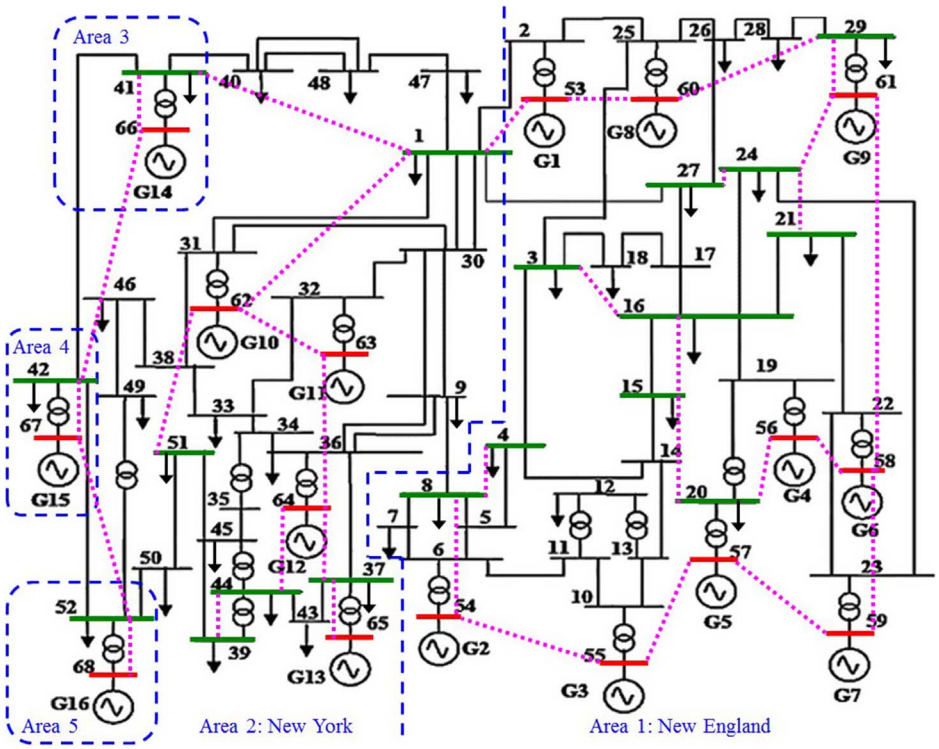

Fig. 1. The New York-New England 68-bus power network used in simulations. Generator buses and controllable load buses are marked in red and green, respectively. The dotted magenta lines represent communication links for the proposed distributed control. (For interpretation of the references to color in this figure legend, the reader is referred to the web version of this article.)

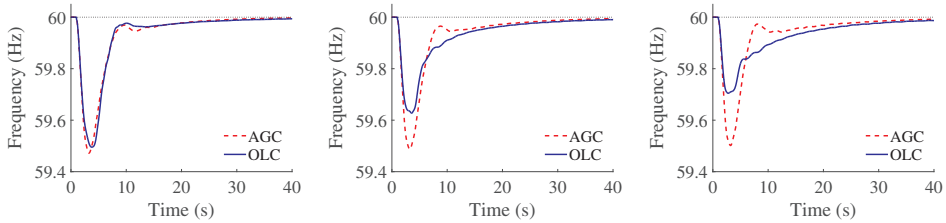

(a) 0% load control (b) 25% load control (c) 50% load control

Fig. 2. Frequency at Bus 62 under different percentages of load control and different control schemes.

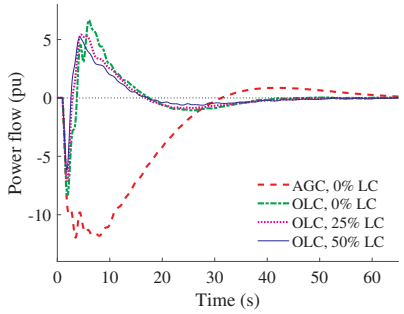

Fig. 3. Deviation of total power flow out of Area 1, under different percentages of load control and different control schemes. Plots for AGC under 25% and 50% load control are not shown because they are similar to the plot for AGC under zero load control.

K^{OLC}, K^{λ}, K^{π}, and B' in OLC and the ACE integral gains in AGC are tuned purposely to make OLC have a comparable dynamic performance to AGC when only the generators participate in frequency regulation. As the percentage of load control increases, the advantage of OLC over AGC in terms of improving the frequency nadir (compared under the same controllable resources, i.e., in the same subfigure of Fig. 2) becomes more significant. Understanding the exact cause of such improvement requires future work, and here is a possible intuitive explanation. The $K_i^{\mathrm{OLC}}\omega_i$ terms for controllable loads in OLC (see Section 6.1) play a similar role to the load-damping terms $D_i\omega_i$ in improving frequency nadir. Note that AGC is based on the integral of frequency and inter-area flow deviations and hence does not add damping; the $K_i^{\mathrm{OLC}}\lambda_i$ terms for both generators and loads in OLC are built up slowly (see Fig. 6); and the $K_i^{\mathrm{OLC}}\omega_i$ terms for generators experience delays to affect power outputs due to relatively slow turbine-governor dynamics. Therefore none of these terms can increase system damping at the beginning stage of the transient as effectively as $K_i^{\mathrm{OLC}}\omega_i$ implemented on loads.

It is also observed from Fig. 2 that OLC with a higher percentage of load control increases frequency settling time. Here is a possible reason. The low frequency nadirs under AGC and 0%-load-control OLC drastically raise generator control commands (the sum of primary and secondary) around 3–5 s, and then significantly increase generator power outputs after the delay of turbine-governor dynamics. This leads to quick restoration of frequency, almost to the extent of overshoot above 60 Hz, around 10 s. In contrast, OLC with a higher percentage of load control improves frequency nadir and thus leads to relatively modest increases in generator power outputs. This makes frequency smoother at the cost of slower convergence and longer settling time. It takes future work to understand (i) whether there is an intrinsic tradeoff in OLC between frequency nadir and settling time, and (ii) what are the factors (e.g., controller gains, topology of communication) affecting the settling time of OLC.

In terms of inter-area power flow, it is observed from Fig. 3 that OLC reduces the maximum deviation and leads to faster convergence than

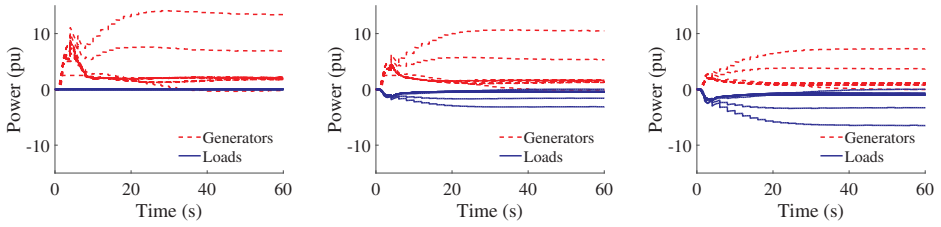

(a) 0% load control (b) 25% load control (c) 50% load control

Fig. 4. Control actions of all the generators and controllable loads under OLC in terms of changes in their power from reference values.

AGC (although the deviation occurs only in one direction under AGC and in both directions under OLC). Moreover, OLC achieves a smaller maximum deviation and faster convergence as the percentage of load control increases.

Fig. 4 shows the control actions of all the generators and controllable loads under OLC in terms of changes in their power from reference values. Specifically, for generators the trajectories of $-K_i^{\mathrm{OLC}}(\lambda_i + \omega_i)$ (which exclude the $+\omega_i/R_i$ terms that cancel the droop control $-\omega_i/R_i$) are plotted, and for controllable loads the trajectories of $K_i^{\mathrm{OLC}}(\lambda_i + \omega_i)$ are plotted. The total steady-state power adjustment of all the generators and controllable loads is approximately (neglecting minor differences in power loss) the same across the cases with 0%, 25%, and 50% load control, and is also approximately the same as the total power imbalance caused by the disturbance. As the percentage of load control increases, the controllable loads contribute more, and correspondingly the generators contribute less, to the total power adjustment. It can be further observed that a higher percentage of load participation helps alleviate the overshoots in generator control actions caused by drastic transient drops in local frequencies.

Fig. 5 shows the voltage magnitudes at Buses 1, 9, 17, 25, 33, 41, 49, 57, 65, under AGC and OLC with different percentages of load control. It is observed that OLC can limit voltage magnitudes within a tighter band than AGC, and also a tighter band under a higher percentage of load control. The voltage magnitudes in transmission systems are typically controlled by automatic voltage regulators (AVRs) which act through generator excitation systems at a faster timescale than frequency control [3]. Same as [9,11,18,21–23], this work essentially assumes that AVRs are capable of maintaining voltage magnitudes within a tight band around the nominal values, so that frequency control can be implemented by purely adjusting active power generations and loads without concerning reactive power and voltages. With increased variations in power imbalance caused by, e.g., higher penetration of non-dispatchable renewable energy, the AVRs may not be adequate to regulate voltages, and enhanced schemes such as joint active and reactive power control of loads may be required. This is an interesting topic for future research.

To illustrate how the computation in the proposed scheme works, the virtual frequency deviations λ_i at all the generators and controllable loads are plotted for the case of OLC with 50% load control, in Fig. 6. It can be observed that λ_i's within each control area converge to the same

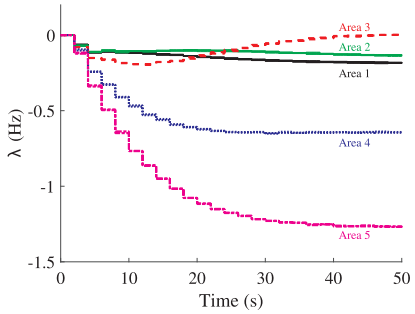

Fig. 6. Virtual frequency deviations λ_i at all the generators and controllable loads under OLC with 50% load control. The plots are grouped in five colors, one for each control area. The λ_i's are updated every two seconds.

value, as predicted by Theorem 2(ii). Fig. 6 also shows that the λ_i's are updated every two seconds, and thus indicates that the proposed scheme can work under a realistic discrete-time implementation.

Furthermore, OLC is tested for two cases of communication link failure. In one case, the communication link connecting Buses 42 and 66 fails; in the other, the failure occurs between Buses 41 and 66. The frequency at Bus 62 and the deviation of total power flow out of Area 4 are plotted for both cases, and compared to the case without communication failure, in Fig. 7. It can be observed that OLC is robust to the tested failures in restoring the nominal frequency. In terms of inter-area power flow, failures of different links lead to different results: When the failure occurs between Buses 42 and 66, which separates the communication graph between Areas 3 and 4, the total power flow out of Area 4 experiences a larger overshoot, but can finally converge to the reference value; when the failure occurs between Buses 41 and 66, which separates the communication graph within Area 3, the total power flow out of Area 4 presents a smaller overshoot but a steady-state error from the reference value. Understanding the impact of different communication link failures will be the subject of future work.

7. Conclusion and future work

We proposed a distributed optimal generator and load control scheme for frequency regulation. After a disturbance in power supply or demand, the proposed scheme can restore the nominal frequency and

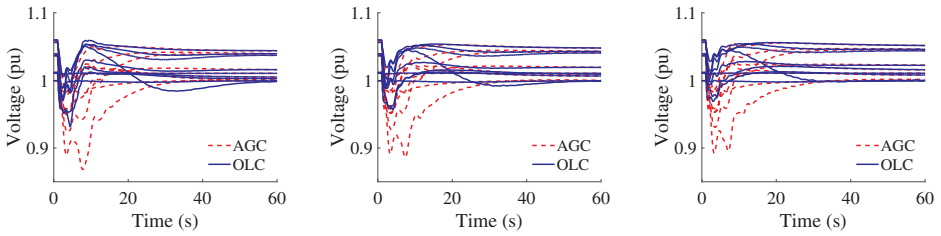

(a) 0% load control (b) 25% load control (c) 50% load control

Fig. 5. Voltage magnitudes at Buses 1, 9, 17, 25, 33, 41, 49, 57, 65, under different percentages of load control and different control schemes.

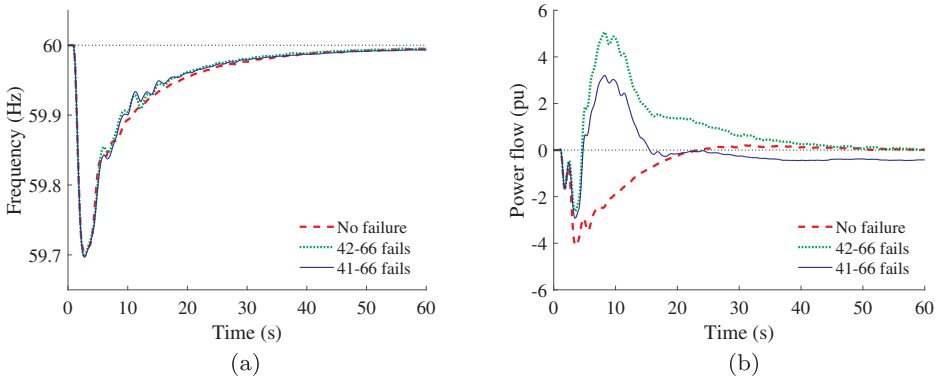

Fig. 7. (a) Frequency at Bus 62 and (b) deviation of total power flow out of Area 4, under different communication link failures. The control scheme is OLC with 50% load control.

the reference inter-area power flows, in a way that minimizes the total cost of control. The proposed scheme is based on local frequency and power flow measurements, local computation, and neighborhood information exchanges over a communication network with an arbitrary (but connected) topology, and is therefore suitable for autonomous and plug-and-play operations. Convergence of the closed-loop system to an optimal equilibrium was proved when a nonlinear power flow model and a generic turbine-governor model were considered; based on that, stability conditions for first- and second-order turbine-governor models were also derived as special cases. Simulation results on a realistic model showed that the proposed control can successfully achieve the frequency regulation goals. Moreover, the proposed control showed a comparable dynamic performance to AGC when implemented only on the generator side, and showed better dynamic characteristics than AGC when more controllable loads participate in each scheme. Robustness of the proposed control to certain communication link failures was also observed in simulations.

This is a proof-of-concept paper that proposes a novel plug-and-play frequency regulation scheme. Further analytical and experimental studies are required to investigate many different aspects of its performance, for example:

- Incorporate other common constraints, such as thermal limits of transmission lines, with frequency regulation. Such a unified frequency regulation and congestion management framework has been developed for a linearized power flow model in [13,14].
- Derive less conservative stability conditions.
- Consider a more realistic power network model, which includes power loss on transmission lines, reactive power flow, dynamics of voltage magnitudes, etc., for controller design and stability analysis.
- Investigate factors that impact dynamic behavior of the system, and design controllers accordingly for better dynamic performance.
- Design controllers, prove stability, and demonstrate controller performance under a sparse placement of controllers, a sparse communication network, and the current SCADA system which transmits electrical and control signals asynchronously on a relatively low time resolution.
- Understand the effect of feedback delay on system stability, and exploit these understandings to guide controller design. Under the proposed control, all the sources of delay, including communication packet loss and packet retransmission, add to the feedback delay of the closed-loop system, which may destabilize the system. Currently, under the assumption of zero feedback delay, the system is proved to be stable with arbitrarily large control gains. In the presence of feedback delay, however, the control gains cannot be too large and may need to be scaled down. Developing guidelines on setting these gains calls for future research effort.
- Based on the observations from Fig. 7, further investigate both analytically and numerically the impact of communication link failure on the proposed control, and obtain guidelines on configuring the communication graph to improve robustness of the proposed control.
- Study scalability of the proposed control, especially in terms of dynamic properties such as convergence speed, for larger networks with more than thousands of controllable loads. An appropriate model that extends the one in Section 2.2 from transmission to distribution networks, and from aggregated to distributed loads, will be required.

Acknowledgment

This work was supported by NSF through grants CNS 1545096, EPCN 1619352, and CCF 1637598, DTRA through grant HDTRA 1-15-1-0003, ARPAE through the GRID DATA program and the NODES program, and Skoltech through Collaboration Agreement 1075-MRA. The work of E. Mallada was also supported by Johns Hopkins E2SHI Seed Grant, ARO through contract W911NF-17-1-0092, and NSF through grants CNS 1544771, EPCN 1711188, and AMPS 1736448.

The U.S. Government retains and the publisher, by accepting the article for publication, acknowledges that the U.S. Government retains a nonexclusive, paid-up, irrevocable, worldwide license to publish or reproduce the published form of this work, or allow others to do so, for U.S. Government purposes.

Appendix A

A.1. Proof of Theorem 1

(Existence.) OLC (5) is convex and satisfies Slater's condition [34, Section 5.2.3], so a point $(p_{\mathscr{G}},d,P)$ is optimal for (5) if and only if it, together with dual variables (λ,π), satisfies the KKT conditions [34, Section 5.5.3]:

(5b)–(5c)

$$p_i = p_i(\lambda_i,0)\,, \quad \forall\, i \in \mathscr{G}, \quad d_i = d_i(\lambda_i,0)\,, \quad \forall\, i \in \mathscr{N} \tag{12}$$

$$\sum_{k\in\mathscr{K}} (E_{ki}-E_{kj})\pi_k = \lambda_i-\lambda_j\,, \quad \forall\, ij \in \mathscr{E} \tag{13}$$

where (5b) and (5c) are primal feasibility and (12) and (13) integrate stationarity, dual feasibility, and complementary slackness. By Lemma 1, in the region where $|\theta_{ij}^*| < \pi/2$ for all $ij \in \mathscr{E}$, there exists a unique $(C^T\theta^*, p_{\mathscr{G}}^*, d^*, P^*)$, such that $(p_{\mathscr{G}}^*, d^*, P^*)$ is optimal for (5) and thus satisfies the KKT conditions with some (λ^*, π^*). Set $\omega^* = 0$. Find $(p_{\mathscr{G}}^{\mathrm{m},*}, a_{\mathscr{G}}^*)$ which is uniquely determined by $g_i(p_i^{\mathrm{m},*}, a_i^*, p_i^*) = 0$ under Assumption 1. Moreover, there is a unique $C'^T\phi^*$ which solves

$$C'B'C'^T\phi^* = r + p^{\mathrm{m},*} - d^* \tag{14}$$

because the kernel of $C'B'C'^T$ is $\mathrm{span}(\mathbf{1}_{\mathscr{N}})$ and $C'^T\mathbf{1}_{\mathscr{N}} = 0$ [35]. It is easy to show that $x^* = (C^T\theta^*, \omega^*, P^*, p_{\mathscr{G}}^{\mathrm{m},*}, a_{\mathscr{G}}^*)$, $u^* = (p_{\mathscr{G}}^*, d^*)$, and $z^* = (\lambda^*, \pi^*, C'^T\phi^*)$ form a solution of (1), (2), (7) where $(\dot\theta, \dot\omega_{\mathscr{G}}, \dot p_{\mathscr{G}}^{\mathrm{m}}, \dot a_{\mathscr{G}}, \dot\lambda, \dot\pi) = 0$ and $\dot\phi_i = \dot\phi_j$ for all $i,j \in \mathscr{N}$, and hence (x^*, u^*, z^*) is an equilibrium of (1), (2), (7). In showing this, we use the fact that (7c) is equivalent to:

$$\dot\lambda_i = K_i^\lambda \left(r_i + p_i^{\mathrm{m}} - d_i - \sum_{j:i\leftrightarrow j} B'_{ij}(\phi_i - \phi_j) \right), \quad \forall\, i \in \mathscr{N}$$

which is obtained by (1b) and (1c).

(Uniqueness.) Consider any equilibrium (x^*, u^*, z^*) of (1), (2), (7). From $(\dot\theta, \dot\omega_{\mathscr{G}}, \dot p_{\mathscr{G}}^{\mathrm{m}}, \dot a_{\mathscr{G}}, \dot\lambda, \dot\pi) = 0$ and $\dot\phi_i = \dot\phi_j$ for all $i,j \in \mathscr{N}$, it is implied that the KKT conditions (5b), (5c), (12), (13) must hold, and hence $(p_{\mathscr{G}}^*, d^*, P^*)$ is optimal for (5). By Lemma 1, the equilibrium $(C^T\theta^*, p_{\mathscr{G}}^*, d^*, P^*)$ is unique in the region where $|\theta_{ij}^*| < \pi/2$ for all $ij \in \mathscr{E}$. The uniqueness of $\omega^* = 0$ is obvious, and the uniqueness of $(p_{\mathscr{G}}^{\mathrm{m},*}, a_{\mathscr{G}}^*)$ results from Assumption 1.

A.2. Proof of Theorem 3

The existence of Y_Θ^*, the uniqueness of (x^*, u^*), and the optimality of $(p_{\mathscr{G}}^*, d^*, P^*)$ are straightforward from Theorem 1. We now prove that $(x(t), u(t)) \to (x^*, u^*)$ as $t \to +\infty$ for every trajectory $(x(t), u(t), z(t))$ of (1), (2), (7) that starts close enough to Y_Θ^*.

Consider an arbitrary $(x(0), u(0), z(0))$ that is close enough to Y_Θ^*, and select an arbitrary z^* such that $(x^*, u^*, z^*) \in Y_\Theta^*$ and z^* is close enough to $z(0)$. Define $(\widetilde x, \widetilde u, \widetilde z) := (x,u,z) - (x^*, u^*, z^*)$. Let $L_{B'} := C'B'C'^T$ denote the Laplacian of the communication network $(\mathscr{N}, \mathscr{E}')$. Consider the energy function

$$U := U_0 + \sum_{i\in\mathscr{G}} U_i$$

where

$$\begin{aligned} U_0 := {} & \tfrac{1}{2}\widetilde\omega_{\mathscr{G}}^T M_{\mathscr{G}} \widetilde\omega_{\mathscr{G}} + \sum_{ij\in\mathscr{E}} B_{ij} \int_{\theta_{ij}^*}^{\theta_{ij}} (\sin\sigma - \sin\theta_{ij}^*) d\sigma \\ & + \tfrac{1}{2}\widetilde\phi^T L_{B'}\widetilde\phi + \tfrac{1}{2}\widetilde\lambda^T (K^\lambda)^{-1}\widetilde\lambda + \tfrac{1}{2}\widetilde\pi^T (K^\pi)^{-1}\widetilde\pi \end{aligned}$$

and U_i satisfies Assumption 4. We have

$$\begin{aligned} \dot U_0 = {} & \widetilde\omega_{\mathscr{G}}^T (r_{\mathscr{G}} + p_{\mathscr{G}}^{\mathrm{m}} - d_{\mathscr{G}} - D_{\mathscr{G}}\omega_{\mathscr{G}} - C_{\mathscr{G}} B \sin(C^T\theta)) \\ & + \widetilde\omega^T (CB\sin(C^T\theta) - CB\sin(C^T\theta^*)) \\ & + (\widetilde\lambda - E^T\widetilde\pi)^T L_{B'}\widetilde\phi + \widetilde\lambda^T (r + p^{\mathrm{m}} - d - L_{B'}\phi) \\ & + \widetilde\pi^T (EL_{B'}\phi - \widehat P_{\mathscr{K}}) \end{aligned} \tag{15}$$

$$\begin{aligned} = {} & \widetilde\omega^T (r + p^{\mathrm{m}} - d - D\omega - CB\sin(C^T\theta^*)) \\ & + \widetilde\lambda^T (r + p^{\mathrm{m}} - d - L_{B'}\phi^*) \\ & + \widetilde\pi^T (EL_{B'}\phi^* - \widehat P_{\mathscr{K}}) \end{aligned} \tag{16}$$

$$= -\widetilde\omega^T D\widetilde\omega - (\widetilde\lambda + \widetilde\omega)^T \widetilde d + (\widetilde\lambda_{\mathscr{G}} + \widetilde\omega_{\mathscr{G}})^T \widetilde p_{\mathscr{G}}^{\mathrm{m}} \tag{17}$$

where (15) results from (1), (7); (16) results from (1c); and (17) results from the definition of equilibrium. Then by (8) we have

$$\begin{aligned} \dot U = {} & \dot U_0 + \sum_{i\in\mathscr{G}} \dot U_i \\ = {} & -\widetilde\omega^T D\widetilde\omega - (\widetilde\lambda_{\mathscr{L}} + \widetilde\omega_{\mathscr{L}})^T \widetilde d_{\mathscr{L}} + \sum_{i\in\mathscr{G}} h_i. \end{aligned} \tag{18}$$

The load control actions d_i are nondecreasing with $(\lambda_i + \omega_i)$ by (7b) and Assumption 2. Moreover, $h_i \leqslant 0$ for all $i \in \mathscr{G}$ by Assumption 4. Therefore $\dot U \leqslant 0$.

Define the set

$$\widetilde Y_\Theta := \{(\widetilde x, \widetilde u, \widetilde z) \mid (x,u,z) \text{ satisfies (1c), (1d), (7a), (7b), and } \widetilde\theta_{ij} \in [-2\theta_{ij}^* - \pi, -2\theta_{ij}^* + \pi],\ \forall\, ij \in \mathscr{E}\}$$

where all the algebraic equations in (1), (2), (7) are satisfied, and for each line $ij \in \mathscr{E}$, the term $\int_{\theta_{ij}^*}^{\theta_{ij}} (\sin\sigma - \sin\theta_{ij}^*) d\sigma$ strictly increases when $\widetilde\theta_{ij}$ deviates further from zero in either direction [28]. We now show that the set

$$\Omega := \{(\widetilde x, \widetilde u, \widetilde z) \in \widetilde Y_\Theta \mid U(\widetilde x, \widetilde u, \widetilde z) \leqslant U(\widetilde x(0), \widetilde u(0), \widetilde z(0))\}$$

is compact and invariant. It is obvious that Ω is a closed set. With $U(\widetilde x, \widetilde u, \widetilde z)$ bounded, the variables $(\widetilde\omega_{\mathscr{G}}, C'^T\widetilde\phi, \widetilde\lambda, \widetilde\pi)$ in Ω are bounded because of the quadratic terms in U_0, and $(\widetilde p_{\mathscr{G}}^{\mathrm{m}}, \widetilde a_{\mathscr{G}})$ are bounded because U_i for $i \in \mathscr{G}$ are radially unbounded (Assumption 4). Moreover, $\widetilde p_{\mathscr{G}}$ and $\widetilde d$ are bounded by $[\underline p_{\mathscr{G}} - p_{\mathscr{G}}^*, \overline p_{\mathscr{G}} - p_{\mathscr{G}}^*]$ and $[\underline d - d^*, \overline d - d^*]$, respectively; $C^T\widetilde\theta$ is bounded by the definition of $\widetilde Y_\Theta$; $\widetilde p$ is bounded by (1d) and the boundedness of $C^T\widetilde\theta$; and $\widetilde\omega_{\mathscr{L}}$ is bounded by (1c) and the boundedness of $(\widetilde d_{\mathscr{L}}, \widetilde p)$. Therefore the set Ω is bounded. Finally, any trajectory $(\widetilde x'(t), \widetilde u'(t), \widetilde z'(t))$ of (1), (2), (7) remains in Ω

for $t \geqslant t_0$ if $(\widetilde{x}'(t_0),\widetilde{u}'(t_0),\widetilde{z}'(t_0)) \in \Omega$, which fulfills the invariance of Ω. This can be shown by checking the conditions below: (i) $\dot{U} \leqslant 0$ so $U(\widetilde{x}'(t),\widetilde{u}'(t),\widetilde{z}'(t)) \leqslant U(\widetilde{x}'(t_0),\widetilde{u}'(t_0),\widetilde{z}'(t_0)) \leqslant U(\widetilde{x}(0),\widetilde{u}(0),\widetilde{z}(0))$ for all $t \geqslant t_0$; (ii) the algebraic equations (1c), (1d), (7a), (7b) are constantly satisfied by $(\widetilde{x}'(t),\widetilde{u}'(t),\widetilde{z}'(t))$; and (iii) for $(x(0),u(0),z(0))$ sufficiently close to (x^*,u^*,z^*) and thus$U(\widetilde{x}(0),\widetilde{u}(0),\widetilde{z}(0))$ sufficiently small, $\widetilde{\theta}'_{ij}(t)$ cannot jump out of$[-2\theta^*_{ij}-\pi,-2\theta^*_{ij}+\pi]$, because $B_{ij}\int_{\theta^*_{ij}}^{\theta^*_{ij}+\widetilde{\theta}'_{ij}(t)}(\sin\sigma-\sin\theta^*_{ij})d\sigma$ is bounded by $U(\widetilde{x}(0),\widetilde{u}(0),\widetilde{z}(0))$.

Define the set

$$Z_\Omega \coloneqq \{(\widetilde{x},\widetilde{u},\widetilde{z}) \in \Omega \mid \dot{U}(\widetilde{x},\widetilde{u},\widetilde{z}) = 0\}$$

and let Z^{I}_Ω denote the largest invariant subset of Z_Ω. Note that $(\widetilde{x}(0),\widetilde{u}(0),\widetilde{z}(0)) \in \Omega$. By LaSalle's theorem [29, Theorem 4.4], $(\widetilde{x}(t),\widetilde{u}(t),\widetilde{z}(t))$ approaches Z^{I}_Ω as $t \to +\infty$. For every $(\widetilde{x},\widetilde{u},\widetilde{z}) \in Z^{\mathrm{I}}_\Omega$, there must be $(\widetilde{\omega},\widetilde{d},\widetilde{p}^{\mathrm{m}}_{\mathscr{G}},\widetilde{a}_{\mathscr{G}}) = 0$ by (18) and Assumption 4, and $(\dot{\omega},\dot{d},\dot{p}^{\mathrm{m}}_{\mathscr{G}},\dot{a}_{\mathscr{G}}) = 0$ since Z^{I}_Ω is invariant. This together with (1b)–(1d) implies $C^T\widetilde{\theta} = 0$ and $\widetilde{p} = 0$, and with Assumption 1 implies $\widetilde{p}_{\mathscr{G}} = 0$. Hence every $(\widetilde{x},\widetilde{u},\widetilde{z}) \in Z^{\mathrm{I}}_\Omega$ satisfies $(\widetilde{x},\widetilde{u}) = 0$, and therefore $(x(t),u(t)) \to (x^*,u^*)$ as $t \to +\infty$, which completes the proof.

A.3. Proof of Theorem 4

The existence of Y^*_Θ, the uniqueness of (x^*,u^*), and the optimality of$(p^*_{\mathscr{G}},d^*,P^*)$ are straightforward from Theorem 1, since the model (3) is a special case of (2) and satisfies Assumption 1. By Theorem 3, it is sufficient for the rest of the proof to show that Assumption 4 holds. Consider:

$$U_i(\widetilde{p}^{\mathrm{m}}_i,\widetilde{a}_i) \coloneqq \frac{\overline{\beta}_i}{2\underline{\beta}_i^{\,2}}(T_{\mathrm{t},i}(\widetilde{p}^{\mathrm{m}}_i)^2 + T_{\mathrm{g},i}(\widetilde{a}_i)^2)\,, \quad \forall\, i \in \mathscr{G}$$

which satisfies conditions (i)–(iii) in Assumption 4. Moreover,

$$\begin{aligned} h_i &= \dot{U}_i + (\widetilde{p}^{\mathrm{m}}_i - \widetilde{d}_i)(\widetilde{\lambda}_i + \widetilde{\omega}_i) \\ &= \frac{\overline{\beta}_i}{\underline{\beta}_i^{\,2}}\left[\widetilde{p}^{\mathrm{m}}_i(-\widetilde{p}^{\mathrm{m}}_i + \widetilde{a}_i) + \widetilde{a}_i\left(-\widetilde{a}_i + \widetilde{p}_i - \frac{\widetilde{\omega}_i}{R_i}\right)\right] \\ &\quad + (\widetilde{p}^{\mathrm{m}}_i - \widetilde{d}_i)(\widetilde{\lambda}_i + \widetilde{\omega}_i) \end{aligned} \tag{19}$$

$$\begin{aligned} &= -\frac{\overline{\beta}_i}{2\underline{\beta}_i^{\,2}}\left[(\widetilde{p}^{\mathrm{m}}_i - \widetilde{a}_i)^2 + \left(\widetilde{p}_i - \frac{\widetilde{\omega}_i}{R_i} - \widetilde{a}_i\right)^2\right] \\ &\quad - \frac{\overline{\beta}_i}{2\underline{\beta}_i^{\,2}}(\widetilde{p}^{\mathrm{m}}_i)^2 + \frac{\overline{\beta}_i}{2\underline{\beta}_i^{\,2}}\left(\widetilde{p}_i - \frac{\widetilde{\omega}_i}{R_i}\right)^2 \\ &\quad + (\widetilde{p}^{\mathrm{m}}_i - \widetilde{d}_i)(\widetilde{\lambda}_i + \widetilde{\omega}_i) \end{aligned} \tag{20}$$

$$\begin{aligned} &\leqslant -\frac{\overline{\beta}_i}{2\underline{\beta}_i^{\,2}}\left[(\widetilde{p}^{\mathrm{m}}_i - \widetilde{a}_i)^2 + \left(\widetilde{p}_i - \frac{\widetilde{\omega}_i}{R_i} - \widetilde{a}_i\right)^2\right] \\ &\quad - \frac{\overline{\beta}_i}{2\underline{\beta}_i^{\,2}}(\widetilde{p}^{\mathrm{m}}_i)^2 + \frac{\overline{\beta}_i}{2\underline{\beta}_i^{\,2}}\underline{\beta}_i^{\,2}(\widetilde{\lambda}_i + \widetilde{\omega}_i)^2 \\ &\quad + (\widetilde{\lambda}_i + \widetilde{\omega}_i)\widetilde{p}^{\mathrm{m}}_i - \overline{\beta}_i(\widetilde{\lambda}_i + \widetilde{\omega}_i)^2 \end{aligned} \tag{21}$$

$$\begin{aligned} &= -\frac{\overline{\beta}_i}{2\underline{\beta}_i^{\,2}}\left[(\widetilde{p}^{\mathrm{m}}_i - \widetilde{a}_i)^2 + \left(\widetilde{p}_i - \frac{\widetilde{\omega}_i}{R_i} - \widetilde{a}_i\right)^2\right] \\ &\quad - \frac{\overline{\beta}_i}{2\underline{\beta}_i^{\,2}}\left(\widetilde{p}^{\mathrm{m}}_i - \frac{\underline{\beta}_i^{\,2}}{\overline{\beta}_i}(\widetilde{\lambda}_i + \widetilde{\omega}_i)\right)^2 \\ &\quad - \frac{\overline{\beta}_i^2 - \underline{\beta}_i^{\,2}}{2\overline{\beta}_i}(\widetilde{\lambda}_i + \widetilde{\omega}_i)^2\,, \quad \forall\, i \in \mathscr{G} \end{aligned}$$

where (19) is obtained by (3), and (21) is obtained by (9). Therefore $h_i \leqslant 0$, and $h_i = 0$ implies $(\widetilde{\lambda}_i + \widetilde{\omega}_i,\widetilde{p}^{\mathrm{m}}_i,\widetilde{a}_i) = 0$ and thus $(\widetilde{d}_i,\widetilde{p}^{\mathrm{m}}_i,\widetilde{a}_i) = 0$. On the other hand, $(\widetilde{d}_i,\widetilde{p}^{\mathrm{m}}_i,\widetilde{a}_i) = 0$ implies $h_i = 0$ by (20). This completes the proof.

A.4. Proof of Theorem 5

For the same reason as in the proof of Theorem 4, it is sufficient to show that Assumption 4 holds for the model (4), under either condition (i) or (ii) in Theorem 5. The internal state vector $\widetilde{a}_i$ is treated as zero-dimensional.

If condition (i) in Theorem 5 holds, consider:

$$U_i(\widetilde{p}^{\mathrm{m}}_i) \coloneqq \frac{\overline{\beta}_i}{2\underline{\beta}_i^{\,2}}T_{\mathrm{t},i}(\widetilde{p}^{\mathrm{m}}_i)^2\,, \quad \forall\, i \in \mathscr{G}$$

which satisfies conditions (i)–(iii) in Assumption 4. Moreover,

$$\begin{aligned} h_i &= \dot{U}_i + (\widetilde{p}^{\mathrm{m}}_i - \widetilde{d}_i)(\widetilde{\lambda}_i + \widetilde{\omega}_i) \\ &= \frac{\overline{\beta}_i}{\underline{\beta}_i^{\,2}}\widetilde{p}^{\mathrm{m}}_i\left(-\widetilde{p}^{\mathrm{m}}_i + \widetilde{p}_i - \frac{\widetilde{\omega}_i}{R_i}\right) + (\widetilde{p}^{\mathrm{m}}_i - \widetilde{d}_i)(\widetilde{\lambda}_i + \widetilde{\omega}_i) \end{aligned} \tag{22}$$

$$= -\frac{\bar{\beta}_i}{2\underline{\beta}_i^2}\left(\widetilde{p}_i - \frac{\widetilde{\omega}_i}{R_i} - \widetilde{p}_i^{\mathrm{m}}\right)^2 - \frac{\bar{\beta}_i}{2\underline{\beta}_i^2}(\widetilde{p}_i^{\mathrm{m}})^2 + \frac{\bar{\beta}_i}{2\underline{\beta}_i^2}\left(\widetilde{p}_i - \frac{\widetilde{\omega}_i}{R_i}\right)^2 + (\widetilde{p}_i^{\mathrm{m}} - \widetilde{d}_i)(\widetilde{\lambda}_i + \widetilde{\omega}_i) \tag{23}$$

$$\leqslant -\frac{\bar{\beta}_i}{2\underline{\beta}_i^2}\left(\widetilde{p}_i - \frac{\widetilde{\omega}_i}{R_i} - \widetilde{p}_i^{\mathrm{m}}\right)^2 - \frac{\bar{\beta}_i}{2\underline{\beta}_i^2}(\widetilde{p}_i^{\mathrm{m}})^2 + \frac{\bar{\beta}_i}{2\underline{\beta}_i^2}\underline{\beta}_i^2(\widetilde{\lambda}_i + \widetilde{\omega}_i)^2 + (\widetilde{\lambda}_i + \widetilde{\omega}_i)\widetilde{p}_i^{\mathrm{m}} - \bar{\beta}_i(\widetilde{\lambda}_i + \widetilde{\omega}_i)^2 \tag{24}$$

$$= -\frac{\bar{\beta}_i}{2\underline{\beta}_i^2}\left(\widetilde{p}_i - \frac{\widetilde{\omega}_i}{R_i} - \widetilde{p}_i^{\mathrm{m}}\right)^2 - \frac{\bar{\beta}_i}{2\underline{\beta}_i^2}\left(\widetilde{p}_i^{\mathrm{m}} - \frac{\underline{\beta}_i^2}{\bar{\beta}_i}(\widetilde{\lambda}_i + \widetilde{\omega}_i)\right)^2 - \frac{\bar{\beta}_i^2 - \underline{\beta}_i^2}{2\bar{\beta}_i}(\widetilde{\lambda}_i + \widetilde{\omega}_i)^2, \quad \forall\, i \in \mathscr{G}$$

where (22) and (24) are obtained by (4) and (10) respectively. Therefore $h_i \leqslant 0$, and $h_i = 0$ implies $(\widetilde{\lambda}_i + \widetilde{\omega}_i, \widetilde{p}_i^{\mathrm{m}}) = 0$ and thus $(\widetilde{d}_i, \widetilde{p}_i^{\mathrm{m}}) = 0$. In the other way, $(\widetilde{d}_i, \widetilde{p}_i^{\mathrm{m}}) = 0$ implies $h_i = 0$ by (23).

If condition (ii) in Theorem 5 holds, consider:

$$U_i(\widetilde{p}_i^{\mathrm{m}}) := \frac{T_{t,i}}{2\beta_i}(\widetilde{p}_i^{\mathrm{m}})^2, \quad \forall\, i \in \mathscr{G}$$

which satisfies conditions (i)–(iii) in Assumption 4. Moreover,

$$h_i = \dot{U}_i + (\widetilde{p}_i^{\mathrm{m}} - \widetilde{d}_i)(\widetilde{\lambda}_i + \widetilde{\omega}_i) = \frac{1}{\beta_i}\widetilde{p}_i^{\mathrm{m}}\left(-\widetilde{p}_i^{\mathrm{m}} + \widetilde{p}_i - \frac{\widetilde{\omega}_i}{R_i}\right) + (\widetilde{p}_i^{\mathrm{m}} - \widetilde{d}_i)(\widetilde{\lambda}_i + \widetilde{\omega}_i) \tag{25}$$

$$= \frac{1}{\beta_i}\widetilde{p}_i^{\mathrm{m}}(-\widetilde{p}_i^{\mathrm{m}} - \beta_i(\widetilde{\lambda}_i + \widetilde{\omega}_i)) + (\widetilde{p}_i^{\mathrm{m}} - \widetilde{d}_i)(\widetilde{\lambda}_i + \widetilde{\omega}_i) \tag{26}$$

$$= -\frac{1}{\beta_i}(\widetilde{p}_i^{\mathrm{m}})^2 - (\widetilde{\lambda}_i + \widetilde{\omega}_i)\widetilde{d}_i, \quad \forall\, i \in \mathscr{G}$$

where (25) and (26) are obtained by (4) and (11) respectively. Therefore $h_i \leqslant 0$, and $h_i = 0$ if and only if $(\widetilde{d}_i, \widetilde{p}_i^{\mathrm{m}}) = 0$ (because $\widetilde{\lambda}_i + \widetilde{\omega}_i = 0$ implies $\widetilde{d}_i = 0$).

References

[1] Liu Q, Ilić MD. Enhanced automatic generation control (E-AGC) for future electric energy systems. Proceedings of IEEE power and energy society general meeting, San Diego, CA, USA. 2012.
[2] Wood AJ, Wollenberg BF. Power generation, operation, and control. 2nd ed. John Wiley & Sons, Inc.; 1996.
[3] Bergen AR, Vittal V. Power systems analysis. 2nd ed. Prentice Hall; 2000.
[4] Kirby BJ. Frequency regulation basics and trends. Tech rep ORNL/TM-2004/291. Oak Ridge National Laboratory; 2004.
[5] Apostolopoulou D, Sauer PW, Domínguez-García AD. Balancing authority area model and its application to the design of adaptive AGC systems. IEEE Trans Power Syst 2016;31(5):3756–64.
[6] Callaway DS, Hiskens IA. Achieving controllability of electric loads. Proc IEEE 2011;99(1):184–99.
[7] Lu N, Hammerstrom DJ. Design considerations for frequency responsive grid friendly™ appliances. Proceedings of IEEE PES transmission and distribution conference and exhibition, Dallas, TX, USA. 2006.
[8] Short JA, Infield DG, Freris LL. Stabilization of grid frequency through dynamic demand control. IEEE Trans Power Syst 2007;22(3):1284–93.
[9] Dörfler F, Simpson-Porco J, Bullo F. Breaking the hierarchy: distributed control and economic optimality in microgrids. IEEE Trans Control Network Syst 2016;3(3):241–53.
[10] Ilić MD. From hierarchical to open access electric power systems. Proc IEEE 2007;95(5):1060–84.
[11] Jokić A, Lazar M, van den Bosch PP. Real-time control of power systems using nodal prices. Int J Electr Power Energy Syst 2009;31(9):522–30.
[12] Zhao C, Topcu U, Li N, Low SH. Design and stability of load-side primary frequency control in power systems. IEEE Trans Autom Control 2014;59(5):1177–89.
[13] Mallada E, Zhao C, Low SH. Optimal load-side control for frequency regulation in smart grids. IEEE Trans Autom Control 2017;62(12):6294–309.
[14] Zhao C, Mallada E, Low SH, Bialek J. A unified framework for frequency control and congestion management. Proceedings of power systems computation conference, Genoa, Italy. 2016.
[15] Li N, Zhao C, Chen L. Connecting automatic generation control and economic dispatch from an optimization view. IEEE Trans Control Network Syst 2016;3(3):254–64.
[16] Wang Z, Liu F, Low SH, Zhao C, Mei S. Distributed frequency control with operational constraints, part I: per-node power balance. IEEE Trans Smart Grid 2017. http://dx.doi.org/10.1109/TSG.2017.2731810.
[17] Wang Z, Liu F, Low SH, Zhao C, Mei S. Distributed frequency control with operational constraints, part II: network power balance. IEEE Trans Smart Grid 2017. http://dx.doi.org/10.1109/TSG.2017.2731811.
[18] Andreasson M, Dimarogonas DV, Sandberg H, Johansson KH. Distributed control of networked dynamical systems: static feedback, integral action and consensus. IEEE Trans Autom Control 2014;59(7):1750–64.
[19] Trip S, Bürger M, De Persis C. An internal model approach to (optimal) frequency regulation in power grids with time-varying voltages. Automatica 2016;64:240–53.
[20] Stegink T, De Persis C, van der Schaft A. A unifying energy-based approach to stability of power grids with market dynamics. IEEE Trans Autom Control 2017;62(6):2612–22.
[21] Zhang X, Papachristodoulou A. A real-time control framework for smart power networks: design methodology and stability. Automatica 2015;58:43–50.
[22] Kasis A, Monshizadeh N, Devane E, Lestas I. Stability and optimality of distributed secondary frequency control schemes in power networks. Available from: arXiv:1703.00532.
[23] Trip S, De Persis C. Distributed optimal load frequency control with non-passive dynamics. IEEE Trans Control Network Syst 2017:43–50. http://dx.doi.org/10.1109/TCNS.2017.2698259.
[24] Zhao C, Mallada E, Low SH. Distributed generator and load-side secondary frequency control in power networks. Proceedings of the conference on information sciences and systems, Baltimore, MD, USA. 2015.
[25] Chow J, Rogers G, Cheung K. Power system toolbox. Cherry Tree Sci Softw 2000;48:53.
[26] Dörfler F, Bullo F. Kron reduction of graphs with applications to electrical networks. IEEE Trans Circ Syst I: Regul Papers 2013;60(1):150–63.
[27] Brooks A, Lu E, Reicher D, Spirakis C, Weihl B. Demand dispatch. IEEE Power Energy Mag 2010;8(3):20–9.
[28] Araposthatis A, Sastry S, Varaiya P. Analysis of power-flow equation. Int J Electr Power Energy Syst 1981;3(3):115–26.
[29] Khalil HK. Nonlinear systems. 3rd ed. Prentice Hall; 2002.
[30] Kasis A, Devane E, Spanias C, Lestas I. Primary frequency regulation with load-side participation—part I: stability and optimality. IEEE Trans Power Syst 2017;32(5):3505–18.
[31] Hatanaka T, Chopra N, Ishizaki T, Li N. Passivity-based distributed optimization with communication delays using PI consensus algorithm. Available from: arXiv:1609.04666.
[32] Canizares C, Fernandes T, Geraldi E, et al. Benchmark models for the analysis and control of small-signal oscillatory dynamics in power systems. IEEE Trans Power Syst 2017;32(1):715–22.
[33] ERCOT concept paper: future ancillary services in ERCOT; 2013. < https://www.ferc.gov/CalendarFiles/20140421084800-ERCOT-ConceptPaper.pdf > .
[34] Boyd SP, Vandenberghe L. Convex optimization. Cambridge University Press; 2004.
[35] Mieghem V. Graph spectra for complex networks. Cambridge University Press; 2011.